Cyclic voltammetry measurements of electroactive surface area of porous nickel: peak current and peak charge methods and diffusion layer effect

Pengcheng Zhu and Yuyuan Zhao

School of Engineering, University of Liverpool, Liverpool L69 3GH, UK

Abstract

Surface area is a key parameter for porous metals for electrode applications. Here we measured the electroactive surface area of porous nickel samples using the cyclic voltammetry peak current and peak charge methods. The peak current method measures the contributions from primary pores, while the peak charge method measures the contributions from both primary and secondary pores. The electroactive surface area measured by both methods decreases with normalised diffusion layer thickness. It follows the semi-infinite model at low normalised diffusion layer thicknesses (<0.35) and the thin-layer model at high normalised diffusion layer thickness (>0.35). The correcting factors obtained from the semi-infinite model provide quantitative information on the pore surface roughness and the secondary porosity contribution. The surface roughness of the samples produced by Lost Carbonate Sintering is 2.15. The relative contribution of secondary porosity depends on the type of porous nickel and increases with scan rate, due to reduced diffusion layer thickness. It is in the range of 0.14-0.3 for the samples produced by Lost Carbonate Sintering and loose sintering, and 0.02-0.05 for the sample produced by electrodeposition, for scan rates in the range of 0.005-0.05 V/s.

Keywords: porous metal, electroactive surface area, cyclic voltammetry, diffusion layer

1. Introduction

The use of porous metals as electrodes or current collectors in energy generation is growing because of their large specific surface area, high mass transfer coefficient and good conductivity [1-5]. Lu and Zhao [6] developed a high-efficiency nickel–iron electrode for water splitting by electrodeposition on a porous Ni matrix. Yang *et al* [7] reported that porous Ni with $Ni(OH)_2$ electrodeposited on the surface had a very high specific capacitance. More recently, Fly *et al* [8, 9] applied porous Ni as flow-fields in polymer exchange membrane fuel cells, resulting in highly improved performance compared to conventional designs. The specific electroactive surface area of porous metals is a key parameter for electrode applications because it determines the amount of reaction site, which in turn determines the rate of chemical reaction and energy generation [10].

Cyclic voltammetry (CV) is one of the most effective electrochemical techniques and has been used for determining the surface area of porous materials [11-14]. Diao *et al* [11] developed a CV peak current method to measure the electroactive surface area of porous copper, based on the linear relation between peak current and the electroactive surface area. They first measured the peak currents of a series of mirror-polished copper plates with known areas. They then measured the peak current of a porous copper sample under the same experimental condition and determined the electroactive surface area from the area-current relation established from the copper plates. Zhu and Zhao [15] further studied the effects of porous structure and morphology on the electroactive surface area of porous copper manufactured by the Lost Carbonate Sintering (LCS) process. The electroactive surface area measured by the peak current method was found to be affected by copper particle size, sintering temperature and chemical etching, in addition to pore size and porosity. It was particularly sensitive to the diffusion layer thickness, which is a function of scan rate. The electroactive surface area nearly doubled when the diffusion layer was decreased from 50 μm to 1 μm [15].

The CV peak current method has some limitations as a surface area measurement technique. It essentially measures the area of the outer contour of the diffusion layer and therefore mainly includes the surface area of large pores and fails to capture the features smaller than the diffusion layer, e.g., small voids in the pore walls [15, 16]. Furthermore, the quantitative relation between surface area and peak current is based on semi-infinite diffusion. If the large pores in the samples are smaller than the diffusion layer, thin-layer diffusion becomes dominant and the relation established from solid plates is no longer applicable to porous samples [12, 16-18]. Although the diffusion layer thickness can be reduced by increasing the scan rate to improve the accuracy of measurement, it is practically difficult to use a scan rate above 0.1 V/s, because the effect of electrolyte resistance will become significant at such a high scan rate.

Tan *et al* [19] applied a CV peak charge method to the measurement of the electroactive surface area of nano-porous gold samples. The peak charge method measures the accumulative charge transferred to the porous electrode up to the peak current (termed peak charge). The peak charge can be obtained by integrating the current-time plot from the start of the potential sweep to the time when peak current is reached. With a known specific charge equivalent, i.e. the amount of charge per unit surface area, the electroactive surface area of the samples can be determined from the peak charge. Tan *et al* [19] assumed a constant specific charge equivalent independent of scan rate. The electroactive surface area of the nano-porous gold samples, obtained using this constant specific charge equivalent, decreased with scan rate. This is contrary to the current understanding that a higher scan rate results in a thinner diffusion layer and therefore a larger electroactive surface area [11, 15], indicating that their method was flawed. In fact, the specific charge equivalent is not a constant and it depends on the scan rate applied. Some modifications are necessary to make the peak charge method a reliable technique for surface area measurements.

Compared with the peak current method, the peak charge method can potentially provide more information [19-21]. It measures surface areas contributing to the electrochemical reaction over the potential sweep from zero up to the point of peak current, while the peak current method measures a single surface area when equilibrium is reached and a stable diffusion layer is established. However, the difference in the electroactive surface areas measured by these two methods has not been clearly

interpreted. The different manifestations of the architecture of the porous structure in the two methods are not well understood.

In this paper, we improved the CV peak charge method, taking into account the effect of scan rate on the specific charge equivalent. We measured the electroactive surface area of three types of porous nickel samples, produced by the LCS, loose sintering and electrodeposition processes, using both the peak current and peak charge methods. We studied how diffusion layer thickness and pore size affect the electroactive surface areas measured by these two methods. Combining these two methods, we are able to differentiate the effects of finer details of the porous structure, namely surface roughness and secondary porosity, on the electroactive surface areas in these two methods. This new approach provides a useful technique to study the porous structure of porous metals, especially those produced by powder metallurgy based methods, at different length scales.

2. Experimental

2.1 Preparation of porous Ni samples

A series of porous Ni samples with three pore size ranges, 250-425 μm, 425-710 μm and 710-1000 μm, and various porosities in the range of 0.53-0.77 were fabricated by the LCS process [22, 23]. The raw materials used to produce the samples were commercially pure spherical Ni powder (Tianjiu Industrial Technology Development Ltd., Changsha, China) with a mean particles size of 25 μm and food grade K_2CO_3 powder (E&E Ltd., Melbourne, Australia) with particle sizes in the range of 250-1500 μm. The K_2CO_3 powder was sieved into three different particle size ranges: 250-425 μm, 425-710 μm and 710-1000 μm. The Ni and K_2CO_3 powders were mixed with a pre-specified volume ratio according to the intended porosity, followed by compaction at 200 MPa and sintering at 950 ℃ for 2 hours. The as-produced porous Ni samples were cut into cylindrical specimens, 6 mm in diameter and 5 mm in thickness, by an electrical discharge machine (Prima E250, ONA Ltd., Bristol, UK). The microstructure of the LCS porous Ni samples is composed of interconnected open pores distributed in a Ni matrix formed by sintered Ni particles (Fig. 1a). The pores have the same shapes and sizes as the K_2CO_3 particles used.

In order to study the effect of pore morphology on the surface area measurements, two additional porous Ni samples produced by different manufacturing methods were also used. One sample was manufactured by loose sintering of a spherical Ni powder with a mean particle size of 75 μm with no additives, at 950℃ for 2 hours. The sample was cut into a 6.1 mm × 6.0 mm × 3.8 mm cuboid. Its microstructure is composed of sintered Ni particles containing small voids between the Ni particles with a pore size in the order of 10 μm and a porosity of 0.50 (Fig. 1b). Another sample was obtained from a commercial supplier. It was manufactured by electrodeposition of Ni onto a polymer foam followed by burn-off of the polymer substrate. The sample was cut into a 6.0 mm × 6.0 mm × 1.7 mm cuboid. It has a high porosity of 0.98 and its microstructure is composed of a network of Ni ligaments with polyhedron cells in the order of 500 μm (Fig. 1c). The cells can hardly be treated as pores, because of the lack of cell walls. For comparison purposes, the sample can be regarded as having a very large pore size.

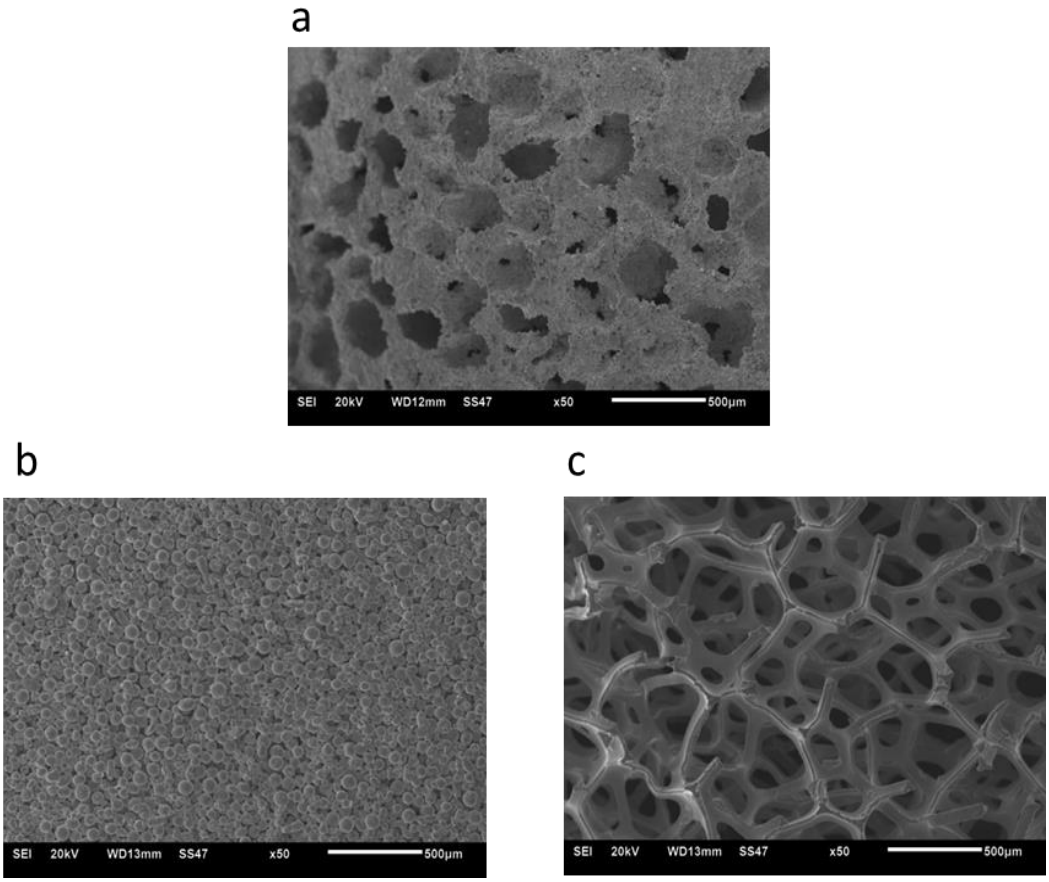

Fig. 1 SEM micrographs of the porous Ni samples manufactured by (a) LCS, (b) loose sintering and (c) electrodeposition processes.

2.2 Preparation of solid Ni plates for calibration

Six solid Ni plates with different exposed surface areas of 1.77, 4.90, 7.84, 10.40, 12.80 and 17.30 mm^2 were used to establish the quantitative relations between electroactive surface area and peak current/peak charge. The Ni plates were ground by silicon carbide papers (from grades 120, 600 to 1200) and then polished by 0.04 μm silk-type cloth pad to a mirror finish before peak current and peak charge measurements. Because of the mirror quality surface finish, the exposed geometric surface areas can be regarded as their electroactive surface areas.

2.3 Pre-treatments

Before electrochemical measurements, the porous and solid Ni specimens were first washed by 10% HCl solution to remove the oxides on the surface and then rinsed in distilled water. Before being transferred to the electrochemical cell, the porous specimens were placed in an agitated sacrificial electrolyte solution to improve the infiltration of electrolyte in the pores.

2.4 Measurements by CV peak current method

A three-electrode electrochemical cell was employed for measuring the electroactive surface area of the porous Ni specimens (for experimental setup details see [11, 15]). A saturated calomel electrode (SCE) reference electrode and a Pt counter electrode (coil for porous specimens or plate for solid specimens) were used, while the porous Ni or solid Ni plate specimen served as the working electrode. The

electrolyte was 1 mM $K_4Fe(CN)_6$ in 0.1 M KOH solution (all chemicals from Sigma Aldrich without further purification). The oxidation reaction of ferrocyanide on the working electrode surface is:

$$[Fe(CN)_6]^{4-} \xrightarrow{oxidation} [Fe(CN)_6]^{3-} + e \quad (1)$$

This reaction is controlled by the diffusion of ferrocyanide ions and has a good reversibility on a Ni surface [24]. Therefore, the peak current is proportional to the electroactive surface area of the working electrode and can be expressed by the Randles-Sevcik equation [25]:

$$I_p = 268600 n^{\frac{3}{2}} A D^{\frac{1}{2}} C v^{\frac{1}{2}} \quad (2)$$

where I_p (A) is the peak current, n is the number of electrons transferred in the redox reaction (n = 1 here), A (cm^2) is the electroactive surface area, D (cm^2/s) is the diffusion coefficient (6×10^{-6} for $[Fe(CN)_6]^{-4}$ [12]), C (mol/cm^3) is the concentration of the reaction species in the electrolyte (10^{-6} for $[Fe(CN)_6]^{-4}$ here) and v (V/s) is the scan rate.

Fig. 2a shows a typical current-potential plot for a LCS porous Ni sample. The current-potential plots for the other porous and solid Ni specimens have similar shapes as that in Fig. 2a. Fig. 2b shows the relations between the peak current and surface area for the solid nickel specimens at three different scan rates, 0.005 V/s, 0.01 V/s and 0.05 V/s. It is shown that the experimental results agree very well with the theoretical predictions from the Randles-Sevcik equation. Assuming that the Randles-Sevcik equation also applies to porous Ni samples, the electroactive surface areas of the porous Ni specimens can be directly calculated using Eq. (2) from the peak currents determined from the current-potential plots.

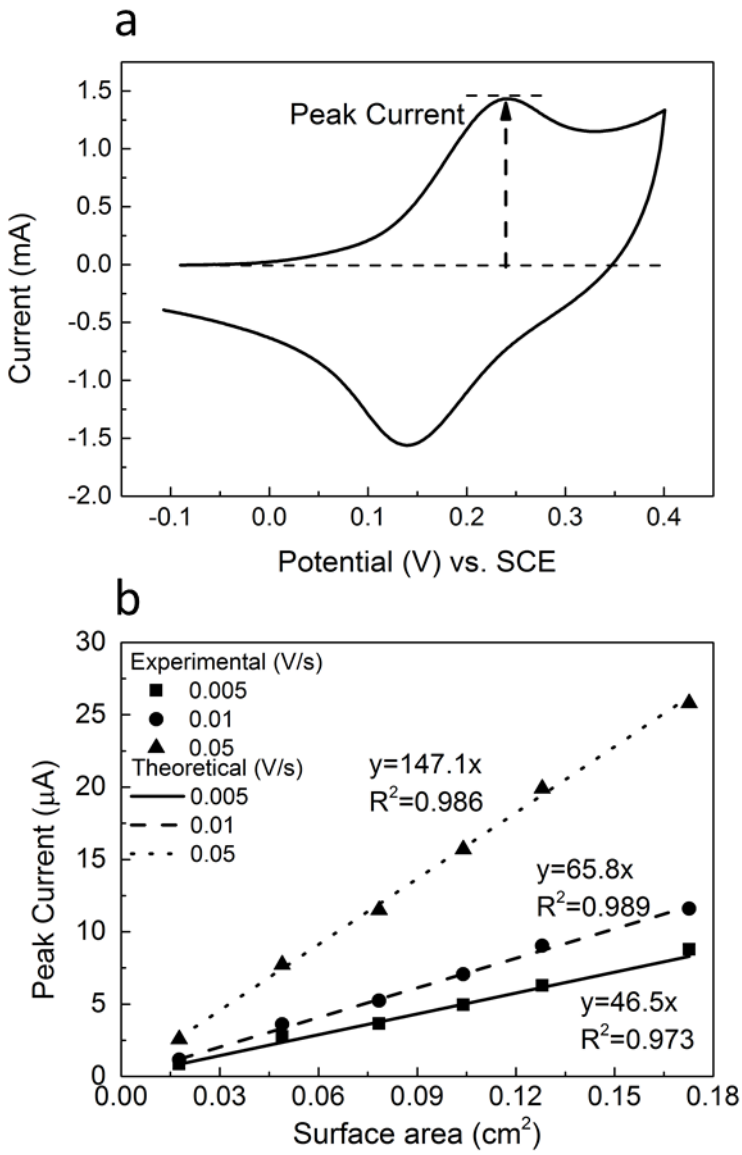

Fig. 2 (a) A typical current-potential plot of the oxidation of ferrocyanide on the surface of a LCS porous Ni sample. (b) Relations between peak current and surface area for solid Ni plates at different scan rates.

2.5 Measurements by CV peak charge method

The same experimental setup and conditions as above were employed in the measurements by the CV peak charge method. For each porous or solid Ni specimen, the current-time plot for the oxidation of ferrocyanide on the working electrode surface, as shown in Fig. 3a, was obtained. The peak charge is the accumulative charge transferred to the electrode before the peak current is reached. It was obtained by integrating current from the start of the potential sweep to the time when peak current was reached and is shown schematically by the hatch area in Fig. 3a.

The relations between peak charge and surface area for the solid Ni specimens at different scan rates are shown in Fig. 3b. It is shown that peak charge is directly proportional to the surface area. The specific charge equivalents, i.e., the peak charge generated per unit surface area [19], are 645.12, 421.95 and 190.97 μC/cm^2 at scan rates of 0.005, 0.01 and 0.05 V/s, respectively. Assuming that the same relations between peak charge and surface area also apply to porous Ni samples, the electroactive surface areas of the porous Ni specimens can be calculated from the peak charge values using the specific charge equivalents obtained from solid Ni specimens.

The peak charge can also be calculated theoretically from the consumption of the ferrocyanide in the electrolyte, which can be estimated by:

$$Q = \frac{1}{2} FA\delta C \tag{3}$$

where, F is Faraday's constant, A is the electroactive surface area, δ is the thickness of the Nernst diffusion layer corresponding to the peak current and C is the concentration of the reaction species in the electrolyte.

The Nernst diffusion layer is the region near the working electrode where the concentration of the electroactive species increases linearly from zero at the working electrode to the bulk concentration of the electrolyte. The diffusion layer thickness at the point of peak current is expressed by [26, 27]:

$$\delta = \frac{nFADC}{I_p} \tag{4}$$

Substituting Eq. (2) into Eq. (4), the Nernst diffusion layer thicknesses at scan rates of 0.005, 0.01 and 0.05 V/s are calculated to be 125, 88 and 39 μm, respectively.

Eq. (3) can be re-arranged to give the specific charge equivalent, i.e., the amount of charge per unit surface area (Q/A), as:

$$Q_{eq} = \frac{1}{2} F\delta C \tag{5}$$

The specific charge equivalent, Q_{eq}, is a function of the Nernst diffusion layer thickness, which varies with scan rate.

The theoretical relations between peak charge and surface area calculated from Eq. 3 for the solid Ni specimens are also shown in Fig. 3b. It is shown that the experimental and theoretical relations agree very well with each other for solid Ni specimens with a flat surface. Therefore, the specific charge equivalents for different scan rates, either calculated from Eq. (5) or determined experimentally from flat solid specimens, can be used to calculate electroactive surface areas of porous samples from peak charges.

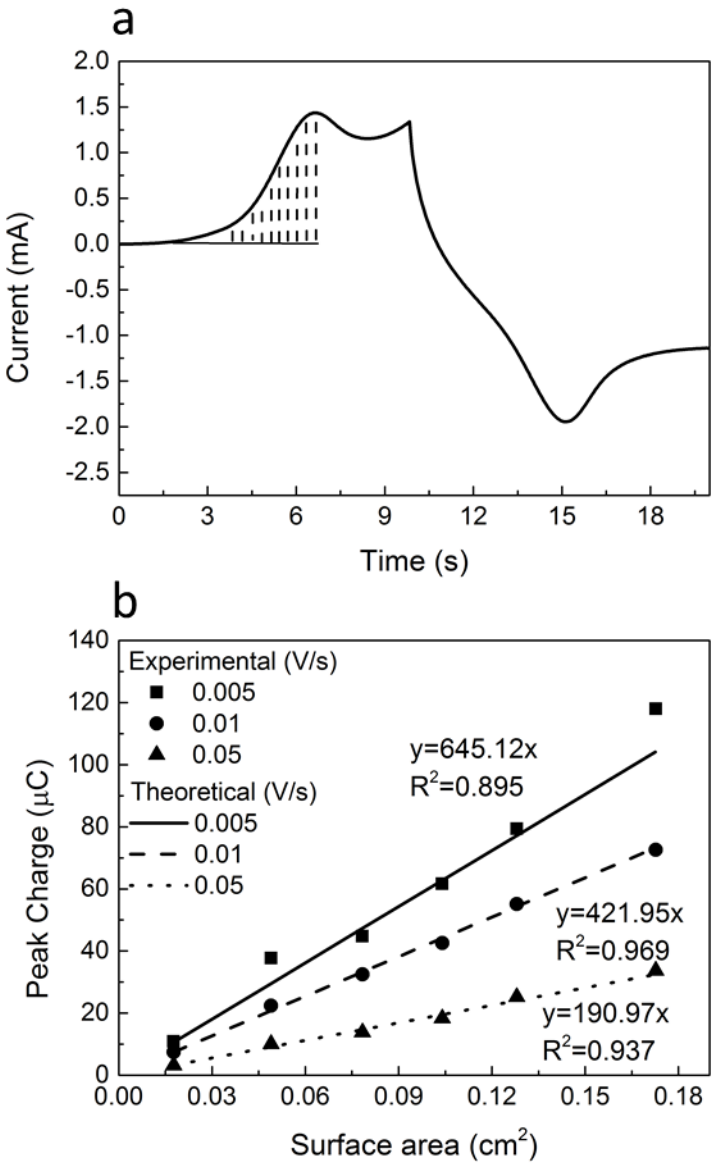

Fig. 3 (a) A typical current-time plot for the oxidation of ferrocyanide on the surface of a LCS porous Ni sample. (b) Experimental and theoretical relations between peak charge and surface area for solid Ni specimens at scan rates of 0.005, 0.01 and 0.05 V/s.

3. Results and Discussion

3.1 Comparison between A_I and A_Q

The volumetric electroactive surface areas obtained by both the peak current and peak charge methods for all the porous Ni samples tested, as well as their pore size and porosity values, are listed in Table 1. Volumetric electroactive surface area, i.e., area per unit volume of porous specimen, is used here to facilitate comparison between different samples. The volumetric electroactive surface areas measured by the CV peak current method, A_I, of the porous Ni specimens are in the range of 27-125 cm^{-1}. A_I increases with porosity and scan rate but decreases with pore size, in agreement with the previous results for porous Cu manufactured by the LCS process [11, 15]. The volumetric electroactive surface areas measured by the CV peak charge method, A_Q, of the porous Ni specimens are in the range of 34-167 cm^{-1}. For each porous Ni specimen, A_Q is 10-30% greater than A_I.

Table 1. Volumetric geometric and electroactive surface areas of porous Ni specimens with different pore sizes and porosities

Process	Pore size (μm)	Porosity	A_G (cm^{-1})	A_I (cm^{-1})			A_Q (cm^{-1})		
				0.005 V/s	0.01 V/s	0.05 V/s	0.005 V/s	0.01 V/s	0.05 V/s
Loose Sintering	~10	0.50	-	30.8	38.8	66.1	35.9	49.4	92.9
LCS	250-425	0.53	60	40.1	51.0	77.3	51.2	69.7	102.9
		0.60	73	38.2	49.1	82.3	50.3	80.7	121.9
		0.62	77	43.6	58.0	92.0	56.3	69.8	122.9
		0.67	82	52.6	71.4	118.9	66.8	86.0	151.9
		0.72	92	54.8	76.5	126.1	61.0	91.9	144.8
		0.77	100	55.1	77.1	125.1	67.9	86.5	166.7
	425-710	0.58	46	37.5	46.5	68.4	46.7	68.3	95.1
		0.62	51	43.0	54.1	84.4	46.4	70.8	123.0
		0.65	54	39.4	51.7	81.2	44.0	65.1	108.6
		0.68	57	39.8	51.2	80.5	46.2	60.4	108.2
		0.72	60	48.3	62.0	92.4	55.1	73.2	116.9
		0.77	64	57.3	72.9	100.7	55.5	84.0	126.2
	710-1000	0.58	30	26.8	34.0	51.6	34.1	46.0	86.4
		0.60	32	31.5	40.9	56.7	34.8	54.3	79.0
		0.69	40	36.9	47.0	72.9	39.5	52.7	94.5
		0.66	38	35.3	43.4	62.1	36.0	54.4	87.8
		0.74	42	42.1	52.4	77.4	39.5	55.9	95.2
		0.75	42	43.5	53.5	78.3	41.6	56.6	104.7
Electro-deposition	-	0.98	-	102.8	111.4	112.5	104.9	115.4	117.3

Fig. 4 shows the relationship between A_Q and A_I. A_Q is approximately proportional to A_I for all the porous Ni specimens. For the LCS and loose sintered specimens, A_Q is greater than A_I by approximately 14%, 22% and 30% when the scan rates were 0.005, 0.01 and 0.05 V/s, respectively. For the electrodeposited specimen, A_Q is greater than A_I by only about 2%, 3% and 4%, corresponding to the scan rates of 0.005, 0.01 and 0.05 V/s. The difference between A_Q and A_I, and the influence of scan rate on the difference can be explained by the porous structure and the effect of diffusion layer thickness.

The electroactive surface area measured by the CV peak charge method is slightly larger than and linearly proportional to the electroactive surface area measured by the CV peak current method. It is because the CV peak current method and the peak charge method measure different electroactive surface areas. The former one measures the electroactive surface area at a particular potential when the Nernst diffusion layer is formed. The electroactive surface area measured by the CV peak current method, A_I, is expected as the contour of the Nernst diffusion layer thickness [15]. For the LCS porous Ni, the size of primary pores is larger than the Nernst diffusion layer thickness and the size of secondary pores is much smaller than the Nernst diffusion layer thickness, so the Nernst diffusion layer only exits within primary pores. Therefore, the electroactive area measured by the CV peak current method includes the surface area of primary pores only and excludes the surface area of secondary pores. The CV peak charge method measures the electroactive surface area in a period from the time when diffusion layer first appears to the time when the full Nernst diffusion layer is formed. When the diffusion layer thickness is extremely thin, not only the primary pores but also the secondary pores can be detected by the peak charge method. Therefore, the electroactive surface area measured by the CV peak charge method includes the contributions from both primary pores and secondary pores. The linear proportionality coefficient between A_I and A_Q increases from 1.14 to 1.22 and further

to 1.30 when the scan rate increases from 0.005 to 0.01 and further to 0.05 V/s, respectively. This is because the contribution of secondary pores increases with increasing scan rate, which will be discussed in Section 3.3.

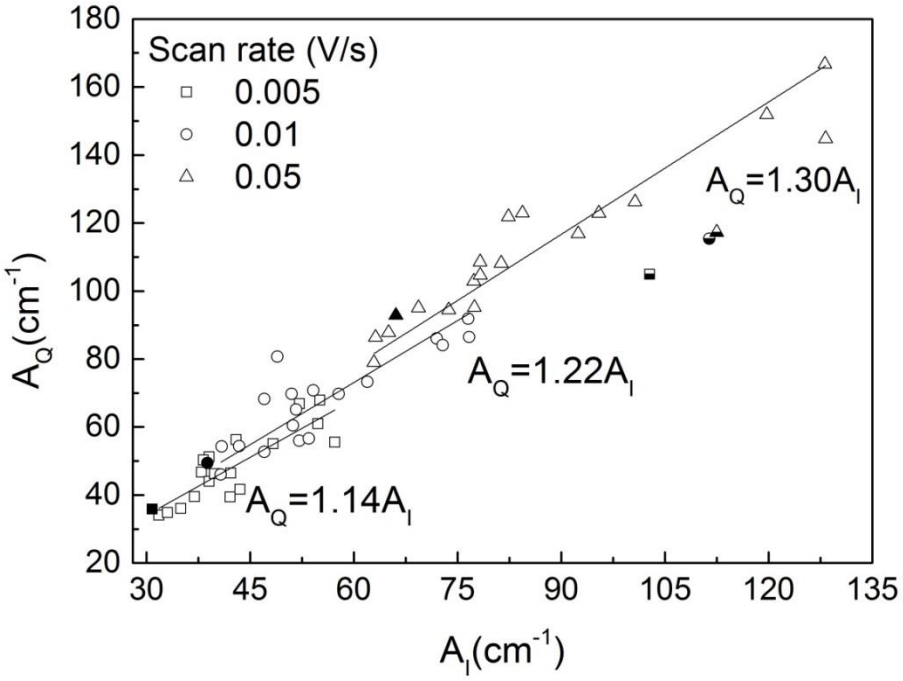

Fig. 4 Relations between the electroactive surface areas measured by the CV peak current method and the CV peak charge method at different scan rates 0.005, 0.01 and 0.05 V/s. (hollow: LCS; solid fill: loose sintered; half solid fill: electrodeposition)

3.2 Effect of diffusion layer thickness with respect to pore size

Fig. 5 shows the ratios of the electroactive surface areas, A_I and A_Q, to the geometric surface area (A_G) as a function of the diffusion layer thickness (δ) with respect to pore radius (R), for the porous Ni samples produced by the LCS process. The geometric surface area of the porous Ni samples was measured by the quantitative stereology method as described in [11], and is listed in Table 1. The diffusion layer thickness was calculated by Eq. (4), i.e., assumed to be the same as that on a flat surface. The pore radius was taken as the geometric mean of the pore size range considered. It is shown that the electroactive to geometric surface area ratios decrease with increasing diffusion layer thickness to pore radius ratio, or normalised diffusion layer thickness (δ/R). Similar trends are observed for both peak current and peak charge cases.

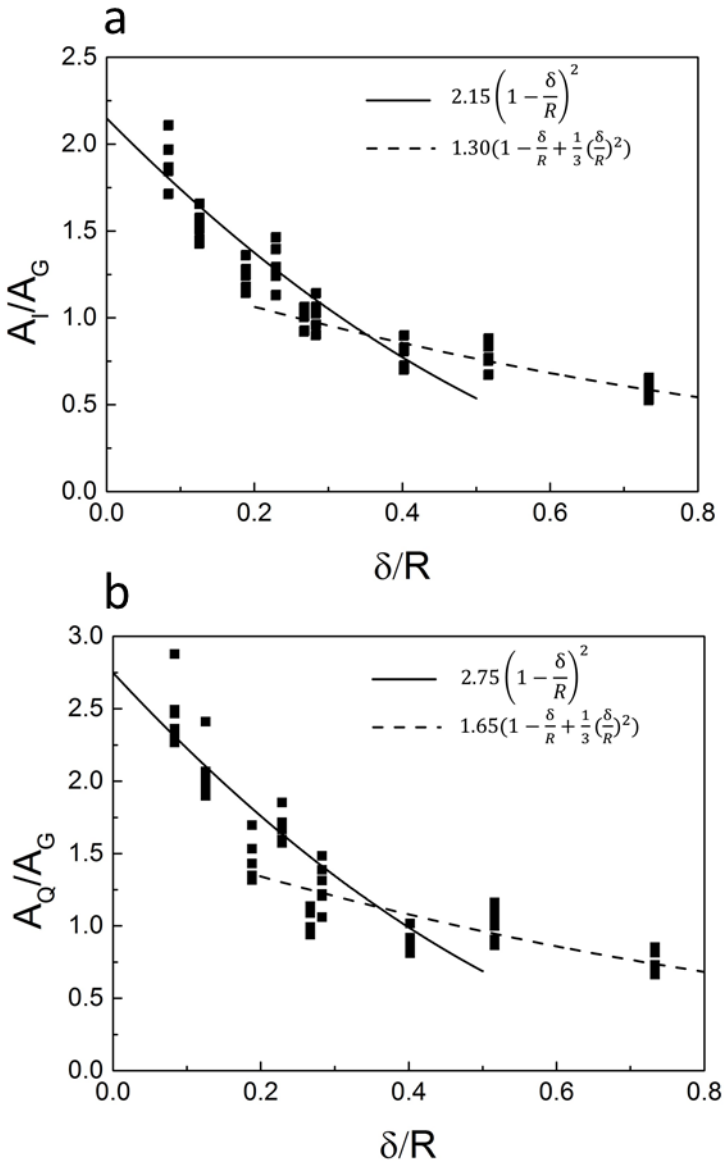

Fig. 5 Ratios of electroactive to geometric surface areas (a) A_I/A_G and (b) A_Q/A_G as a function of normalised diffusion layer thickness, δ/R. (A_I: electroactive surface area measured by the peak current method, A_Q: electroactive surface area measured by the peak charge method, A_G: geometric surface area, δ: diffusion layer thickness and R: pore radius)

To understand how diffusion layer thickness affects the electroactive to geometric surface area ratios, let us consider a perfectly spherical and smooth pore with a radius of R, and a diffusion layer inside the pore with a thickness of δ, as shown schematically in Fig. 6. Assuming that the pore is isolated and not interconnected to other pores, the geometric surface area of the pore is simply the surface area of the sphere, $A_G' = 4\pi R^2$. Two idealised models, semi-infinite and thin-layer diffusion models, can be developed to estimate the electroactive surface area.

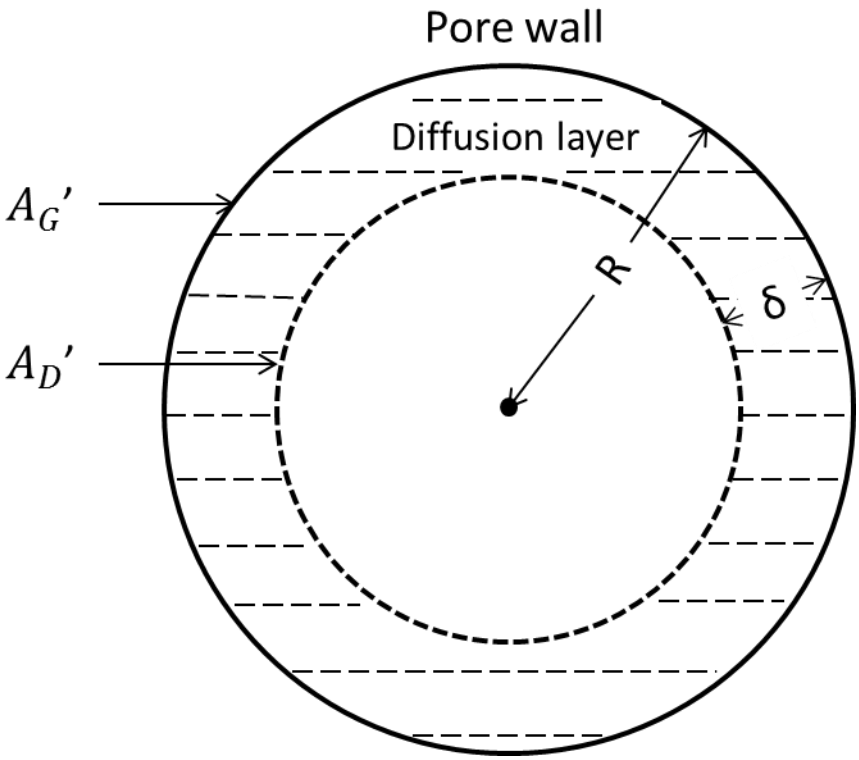

Fig. 6 Schematic diagram showing the diffusion layer inside a spherical pore.

In the semi-infinite diffusion model, the diffusion layer is considered to be much smaller than the pore radius and account for a small proportion of the electrolyte reservoir, so that the concentration of the reaction species in the electrolyte beyond the diffusion layer remains a constant during the measurement. The electroactive surface area of the spherical pore, A_E', can be considered as the surface area of the inner contour of the diffusion layer [15], which can be calculated by:

$$A_E' = A_D' = 4\pi(R-\delta)^2 = A_G'(1-\frac{\delta}{R})^2 \tag{6}$$

In the thin-layer diffusion model, the diffusion layer is considered to be comparable to the pore radius and account for a large part or whole of the electrolyte reservoir. The electroactive surface area can be determined from the amount of reactant consumed, which can be calculated from the concentration of the reactant in the diffusion layer and the volume of the diffusion layer. Assuming that the mean concentration of the reactant in the diffusion layer is half of the concentration outside the diffusion layer (which is true for a large flat electrode and approximately true for an electrode with a small curvature), the total consumption of charge, or peak charge for the spherical pore, Q_t, can be estimated by:

$$Q_t = \frac{1}{2}FC\left[\frac{4}{3}\pi R^3 - \frac{4}{3}\pi(R-\delta)^3\right] = \frac{1}{2}FC\delta A_G'\left[1-\frac{\delta}{R}+\frac{1}{3}\left(\frac{\delta}{R}\right)^2\right] \tag{7}$$

Given the specific charge equivalent in Eq. (5), the electroactive specific surface area of the pore can be determined by:

$$A_E' = \frac{Q_t}{Q_{eq}} = A_G'\left[1-\frac{\delta}{R}+\frac{1}{3}\left(\frac{\delta}{R}\right)^2\right] \tag{8}$$

Eqs. (7) and (8) cannot be applied directly to the porous Ni, because they are developed for isolated spherical and smooth pores. However, the ratio between the electroactive and geometric areas of

porous Ni is expected to be a function of the normalised diffusion layer thickness alone and can still be expressed in the forms of Eqs. (7) and (8), if some simple corrections are applied. Considering that the ratio between the electroactive and geometric areas is equal to the ratio between their volumetric counterparts, the semi-infinite model for porous Ni can be expressed as:

$$\frac{A_E}{A_G} = \frac{A_E'}{A_G'} = S(1 - \frac{\delta}{R})^2 \tag{9}$$

and the thin-layer model as:

$$\frac{A_E}{A_G} = \frac{A_E'}{A_G'} = T\left[1 - \frac{\delta}{R} + \frac{1}{3}\left(\frac{\delta}{R}\right)^2\right] \tag{10}$$

where S and T are constants dependent on the structures of the porous Ni samples and the measurement methods.

Fig. 5 shows that the experimental data for the volumetric electroactive-geometric area ratios, A_I/A_G and A_Q/A_G, fit well with either Eq. (9) or (10) with the introduction of correcting factors S_I = 2.15, S_Q = 2.75, T_I = 1.30 and T_Q = 1.65, where the subscripts I and Q denote the peak current and peak charge methods respectively. The transition occurs at a normalised diffusion layer thickness δ/R = 0.35 for both the peak current and peak charge measurements. In other words, when the diffusion layer is thinner than about one-third of the pore radius, semi-infinite diffusion is dominant and the semi-infinite model works well. When the diffusion layer is thicker than one-third of the pore radius, thin-layer diffusion becomes important and the thin-layer model can be used to describe the electroactive surface area.

3.3 Contributions from surface roughness and secondary pores

The correcting factors (S_I, S_Q, T_I and T_Q) reflect the differences between the measured electroactive surface area of a real porous structure and the theoretical electroactive surface area for an idealised porous structure with spherical and smooth pores. They are therefore useful indicators of the pore surface conditions, including pore sphericity, surface roughness, secondary porosity and inter-connectivity between the pores. Because pore sphericity and inter-pore connecting channels equally affect both geometric and electroactive surface areas, the correcting factors are good indicators of the surface roughness and secondary porosity and their contributions to the electroactive surface area.

As discussed previously, the electroactive surface area measured by the CV peak current method, A_I, is mainly the surface area of the primary pores. The correcting factor for the peak current method, S_I, is accordingly the ratio between the electroactive and geometric areas of the primary pores when the diffusion layer thickness approaches zero. Therefore, S_I provides a direct measurement of the surface roughness and is effectively surface roughness. An S_I value of 2.15 indicates that the maximum electroactive surface area is 2.15 times of the geometric surface area for the porous Ni samples. This agrees with the surface morphology of the porous Ni samples produced by a sintering process. A pore surface formed by the sintering of numerous small metal particles is composed of many half particles close to semi-spheres, each of which has a surface area approximately twice the cross-sectional area. As the former represents the electroactive surface area and the latter signifies the geometric surface area, the ratio between the electroactive and geometric surface areas is expected to be close to two.

The earlier discussion also explained that the electroactive surface area measured by the CV peak charge method, A_Q, includes the contributions from both primary and secondary pores. The difference between S_Q and S_I characterises the difference between A_Q and A_I when the diffusion layer thickness approaches zero and is therefore a good quantitative indicator of the contribution of secondary pores to the electroactive surface area. The relative contribution of secondary pores, or the ratio between the secondary and primary porosity contributions, can be conveniently determined by:

$$\eta = \left(\frac{S_Q}{S_I} - 1\right) \tag{11}$$

For the porous Ni samples produced by the LCS process, the ratio between the secondary and primary porosity contributions is ŋ = 0.28. In other words, the contribution of secondary porosity to the electroactive surface area is 28% of the contribution of the primary porosity. It demonstrates that the secondary porosity contribution is significant and cannot be neglected.

It should be noted that the correcting factor for the thin-layer model by the peak current method, T_I, cannot be directly used to describe surface roughness. This is because the thin-layer condition is only applicable to low scan rates or small pores and cannot be extended to the ideal case when diffusion layer thickness approaches zero. However, it is interesting to observe that, for the LCS porous Ni samples, $T_Q/T_I \approx S_Q/S_I$. It means that the correcting factors for the thin-layer model, T_Q and T_I, are also directly related to the pore surface conditions and the ratio between T_Q and T_I, is also an indicator of the relative contribution of secondary porosity to electroactive surface area, η.

3.4 Behaviours of different types of porous Ni

Although the relation between the normalised area and normalised diffusion layer thickness, as shown in Fig. 5, can be used to differentiate semi-infinite diffusion and thin-layer diffusion, a more direct and intuitive way to reveal the nature of the diffusion regime is to examine the relation between peak current and scan rate. If the slope of the logarithmic current-scan rate curve is 0.5, i.e., the peak current is proportional to the square root of scan rate, the electrochemical reaction is controlled by semi-infinite diffusion. If the slope of the logarithmic current-scan rate curve is 1, then the reaction is controlled by perfect thin-layer diffusion [12, 16].

Fig. 7 shows the relations between volumetric peak current and scan rate in logarithmic scale for the three types of porous Ni samples. The volumetric peak current, which is the peak current divided by the volume of the porous Ni sample, is used here to facilitate comparison. The logarithmic current-scan rate curve for the LCS Ni sample, with a porosity of 0.72 and a pore size of 425-710 μm, shows two linear segments. At high scan rates (thin diffusion layer), the slope of the line is 0.5 and semi-infinite diffusion predominates. At low scan rates (thick diffusion layer), the slope of the line changes to 0.85, entering a partial thin-layer diffusion regime. The current-scan rate curve for the porous Ni sample manufactured by electrodeposition has a slope of 0.5, indicating semi-infinite diffusion control in the full range of scan rates studied. The current-scan rate curve for the porous Ni sample manufactured by loose sintering has a slope of 0.85 in the full range of scan rates studied. This is the same value as that of the LCS sample at low scan rates, indicating partial thin-layer diffusion.

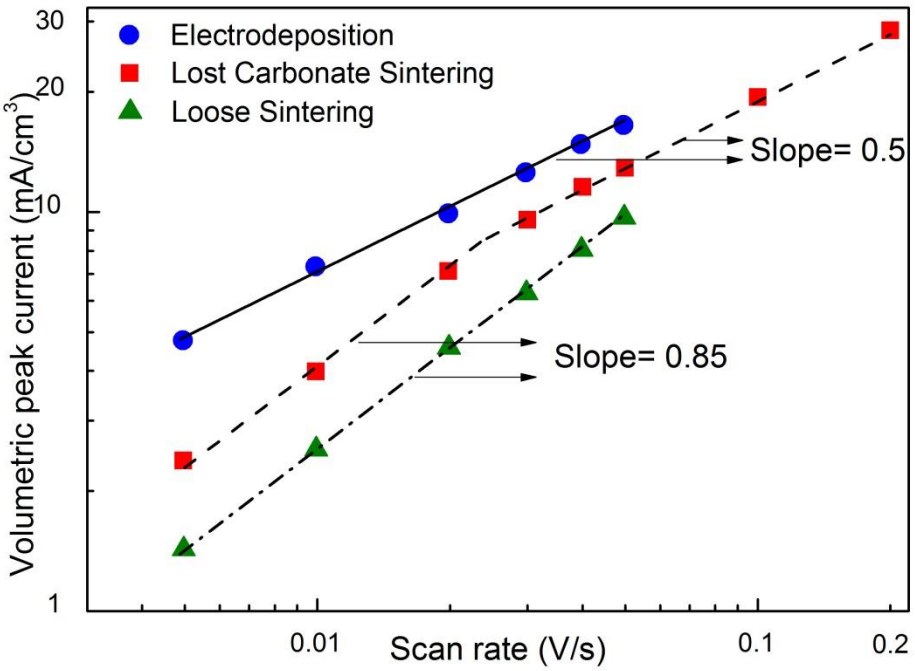

Fig. 7 Logarithmic relations between volumetric peak current and scan rate for different types of porous Ni samples.

The different behaviours among the three types of porous Ni samples are due to their different microstructures (Fig. 1). The porous structure produced by the electrodeposition process is a network of thin struts with high porosity. It can be regarded as composed of large pores, or small normalised diffusion layer thickness, δ/R. As a consequence, semi-infinite diffusion predominates. On the contrary, the porous structure produced by the loose sintering process consists of many small pores relative to the diffusion layer, or large δ/R. Thin-layer diffusion is the predominant condition. The porous structure of the LCS sample has intermediate pore sizes. The normalised diffusion layer thickness, δ/R, can be small or large, depending on the scan rate. As a result, either semi-infinite or partial thin-layer diffusion can be in operation.

It is evident from Fig. 4 that the LCS and loose sintered porous Ni samples have the same ratio of A_Q to A_I at the same scan rate, indicating similar secondary porosity contribution to the electroactive surface area. This is somewhat expected as they are both produced by sintering and have similar microstructural characteristics. The only difference lies in the different pore size and porosity. The ratio of A_Q to A_I for the porous Ni sample produced by electrodeposition, however, is clearly lower than that of the LCS and loose sintered porous Ni samples at the same scan rate. In fact, A_Q is greater than A_I by only 2-5%. It means that the porous Ni sample produced by electrodeposition has less secondary porosity contribution to the electroactive surface area than the LCS and loose sintered porous Ni samples. Again, this is not a surprise as the deposition process produces metal struts with much less internal voids than a sintered metal.

4. Conclusions:

The CV peak current and peak charge methods were employed to measure the electroactive surface area of porous Ni. The two methods measure the electroactive surface areas at different length scales. The peak current method measures the contributions from primary pores, while the peak charge method measures the contributions from both primary and secondary pores. Combining the two methods provides a technique to determine the pore surface roughness and the relative contribution of secondary porosity to electroactive surface area.

The ratio of electroactive surface area to geometric surface area decreases with normalised diffusion layer thickness. The relation follows the semi-infinite model at low normalised diffusion layer thicknesses (<0.35) and the thin-layer model at high normalised diffusion layer thicknesses (>0.35). The correcting factor obtained from the semi-infinite model for the peak current method, S_I, provides a direct measurement of pore surface roughness. The porous Ni samples produced by the LCS process have a surface roughness of 2.15. The ratio between the correcting factors obtained from the semi-infinite model for the peak charge and peak current methods, S_Q/S_I, can be used to quantify the contribution of secondary porosity to the electroactive surface area. The relative contributions of secondary porosity are 0.14, 0.22 and 0.30 for the porous Ni samples produced by LCS and loose sintering, and 0.02, 0.03 and 0.04 for the porous Ni sample produced by electrodeposition, at the scan rates of 0.005, 0.01 and 0.05 V/s, respectively.

References

[1] M.F. Ashby, T. Evans, N.A. Fleck, J. Hutchinson, H. Wadley, L. Gibson, Metal Foams: A Design Guide: A Design Guide, Elsevier, 2000.
[2] P. Cognet, J. Berlan, G. Lacoste, P.-L. Fabre, J.-M. Jud, Application of metallic foams in an electrochemical pulsed flow reactor Part I: Mass transfer performance, J. Appl. Electrochem., 25 (1995) 1105-1112.
[3] J. Banhart, Manufacture, characterisation and application of cellular metals and metal foams, Prog. Mater Sci., 46 (2001) 559-632.
[4] P. Liu, K. Liang, Review Functional materials of porous metals made by P/M, electroplating and some other techniques, J. Mater. Sci., 36 (2001) 5059-5072.
[5] L.P. Lefebvre, J. Banhart, D.C. Dunand, Porous metals and metallic foams: current status and recent developments, Adv. Eng. Mater., 10 (2008) 775-787.
[6] X. Lu, C. Zhao, Electrodeposition of hierarchically structured three-dimensional nickel–iron electrodes for efficient oxygen evolution at high current densities, Nat. Commun., 6 (2015) 6616.
[7] G. Yang, C. Xu, H. Li, Electrodeposited nickel hydroxide on nickel foam with ultrahigh capacitance, Chem. Commun., (2008) 6537-6539.
[8] A. Fly, D. Butcher, Q. Meyer, M. Whiteley, A. Spencer, C. Kim, P. Shearing, D.J. Brett, R. Chen, Characterisation of the diffusion properties of metal foam hybrid flow-fields for fuel cells using optical flow visualisation and X-ray computed tomography, J. Power Sources, 395 (2018) 171-178.
[9] A. Fly, Q. Meyer, M. Whiteley, F. Iacoviello, T. Neville, P. Shearing, D.J. Brett, C. Kim, R. Chen, X-ray tomography and modelling study on the mechanical behaviour and performance of metal foam flow-fields for polymer electrolyte fuel cells, Int. J. Hydrogen Energy, 44 (2019) 7583-7595.
[10] C. Brett, M.O. Brett, A.M.C.M. Brett, A.M.O. Brett, Electrochemistry: principles, methods, and applications, 1993.
[11] K.K. Diao, Z. Xiao, Y.Y. Zhao, Specific surface areas of porous Cu manufactured by Lost Carbonate Sintering: Measurements by quantitative stereology and cyclic voltammetry, Mater. Chem. Phys., 162 (2015) 571-579.
[12] R.E. Smith, T.J. Davies, N.d.B. Baynes, R.J. Nichols, The electrochemical characterisation of graphite felts, J. Electroanal. Chem., 747 (2015) 29-38.

[13] J.M.D. Rodríguez, J.A.H. Melián, J.P. Peña, Determination of the real surface area of Pt electrodes by hydrogen adsorption using cyclic voltammetry, J. Chem. Educ, 77 (2000) 1195.
[14] M. Grdeń, M. Alsabet, G. Jerkiewicz, Surface science and electrochemical analysis of nickel foams, ACS Appl. Mater. Interfaces, 4 (2012) 3012-3021.
[15] P. Zhu, Y. Zhao, Effects of electrochemical reaction and surface morphology on electroactive surface area of porous copper manufactured by Lost Carbonate Sintering, RSC Adv., 7 (2017) 26392-26400.
[16] E.O. Barnes, X. Chen, P. Li, R.G. Compton, Voltammetry at porous electrodes: A theoretical study, J. Electroanal. Chem., 720 (2014) 92-100.
[17] T.J. Davies, R.G. Compton, The cyclic and linear sweep voltammetry of regular and random arrays of microdisc electrodes: Theory, J. Electroanal. Chem., 585 (2005) 63-82.
[18] T.J. Davies, S. Ward-Jones, C.E. Banks, J. del Campo, R. Mas, F.X. Munoz, R.G. Compton, The cyclic and linear sweep voltammetry of regular arrays of microdisc electrodes: fitting of experimental data, J. Electroanal. Chem., 585 (2005) 51-62.
[19] Y.H. Tan, J.A. Davis, K. Fujikawa, N.V. Ganesh, A.V. Demchenko, K.J. Stine, Surface area and pore size characteristics of nanoporous gold subjected to thermal, mechanical, or surface modification studied using gas adsorption isotherms, cyclic voltammetry, thermogravimetric analysis, and scanning electron microscopy, J. Mater. Chem., 22 (2012) 6733-6745.
[20] T.J. Davies, Anodic stripping voltammetry with graphite felt electrodes for the trace analysis of silver, Analyst, 141 (2016) 4742-4748.
[21] A. Pozio, M. De Francesco, A. Cemmi, F. Cardellini, L. Giorgi, Comparison of high surface Pt/C catalysts by cyclic voltammetry, J. Power Sources, 105 (2002) 13-19.
[22] Y. Zhao, T. Fung, L. Zhang, F. Zhang, Lost carbonate sintering process for manufacturing metal foams, Scripta Mater., 52 (2005) 295-298.
[23] L. Zhang, Y. Zhao, Fabrication of high melting-point porous metals by lost carbonate sintering process via decomposition route, Proc. Inst. Mech. Eng. B J. Eng. Manuf., 222 (2008) 267-271.
[24] Z. Gao, L. Chen, J. Chang, Z. Wang, D. Wu, F. Xu, K. Jiang, Bare Ni foam electrode-ferricyanides redox electrolyte system with high capacitive performance, Int. J. Hydrogen Energy, (2019).
[25] C. Brett, A.M. Oliveira Brett, Electrochemistry: principles, methods, and applications, Oxford University Press, Oxford, 1993.
[26] C. Amatore, S. Szunerits, L. Thouin, J.-S. Warkocz, The real meaning of Nernst's steady diffusion layer concept under non-forced hydrodynamic conditions. A simple model based on Levich's seminal view of convection, J. Electroanal. Chem., 500 (2001) 62-70.
[27] A. Molina, J.n. González, F. Martínez-Ortiz, R.G. Compton, Geometrical insights of transient diffusion layers, J. Phys. Chem. C, 114 (2010) 4093-4099.

Author contributions

Zhu conducted the experiments and wrote the manuscript. Zhao supervised the whole work and contributed to the analysis, interpretation and presentation of results.